Finding Boundary Conditions: A Coupling Strategy for the Modeling of Metal Casting Processes: Part I. Experimental Study and Correlation Development

MICHAEL TROVANT and STAVROS ARGYROPOULOS

A generalized temperature boundary condition coupling strategy for the modeling of conventional casting processes was implemented *via* experiments and numerical simulations with commercial purity aluminum, aluminum alloy, and tin specimens in copper, graphite, and sand molds. This novel strategy related the heat transfer coefficient at the metal-mold interface to the following process variables: the size of the air gap that forms at the metal-mold interface, the roughness of the mold surface, the conductivity of the gas in the gap, and the thermophysical properties of both the metal and mold. The objective of this study was to obtain, apply, and evaluate the effect of incorporating an experimentally derived relationship for specifying transient heat transfer coefficients in a general conventional casting process. The results are presented in two parts. Part I details the implementation of a systematic experimental approach not limited to a specific process to determine the heat transfer coefficient and characterize the formation of the air gap at the metal-mold interface. The heat transfer mechanisms at the interface were identified, and seen to vary in magnitude during four distinct stages, as the air gap formed and grew. A semiempirical inverse equation was used to characterize the heat transfer coefficient–air gap relationship, across the various stages, for experimental data from the literature and this study.

I. INTRODUCTION

A moderate change in the boundary conditions imposed at the metal-mold interface in many casting simulations can severely affect the validity of the resulting numerical predictions. This is especially evident with temperature boundary conditions defined by heat transfer coefficients for a number of reasons. First, temperature boundary conditions are inherently transient during most commercial casting processes. Heat transfer coefficients are initially high and tend to drop off at lower temperatures. Second, not one, but several mechanisms of heat transfer occur at the metal-mold interface during solidification and cooling, some of which may or may not be present at any given time. In addition, the specification of a temperature boundary condition is highly dependent on the casting and mold configuration. For instance, certain metal-mold interfaces will remain in contact, while others will develop extensive air gaps depending on their orientation with respect to gravity. Finally, heat transfer coefficients are very sensitive to both mold and metal materials and the surface characteristics of each. If one wishes to minimize these errors, the next step toward unification of the complex phenomena associated with modeling casting processes is the coupling of boundary conditions among all related governing equations in a given system. The proper definition of temperature boundary conditions hinges on determining the effect on boundary conditions of certain process variables dictated by coupled governing phenomena.

Accurate heat transfer coefficients are historically difficult to obtain experimentally for all points on the metal-mold interface, especially when the influence of thermal contraction is acknowledged. The main focus of this study is an attempt to remedy some of the pitfalls associated with the specification of heat transfer boundary conditions at the outer boundary of the metal. The ultimate goal is to allow the modeler to estimate the effect of changes in the heat loss at the metal-mold interface, and ultimately to allow the time-dependent heat transfer coefficient for a particular metal-mold system to be assessed *via* a numerical correlation, without resorting to a specific experiment. To achieve this goal, the processes that take place at the metal-mold interface need to be examined. More specifically, the transient mechanisms of heat transfer at the interface and the formation of the air gap between metal and mold must be understood.

Part I of this study will focus on the following experimental issues:

(1) to develop an experimental technique to characterize the formation of the air gap at the metal-mold interface during casting;
(2) to develop and refine a unique experimental technique to determine the heat transfer coefficient at the same metal-mold interface;
(3) to take a systematic approach (not limited to a specific casting process) to quantify the heat transfer coefficient–air gap/thermophysical property/surface roughness relationship across a varying range of metal-mold systems;
(4) to correlate the heat transfer coefficient–air gap relationship using a semiempirical for all systems, including data available in the literature; and
(5) to quantify the error in heat transfer coefficient and air gap measurements.

MICHAEL TROVANT, formerly Graduate Student, Department of Metallurgy and Materials Science, University of Toronto, is Process Engineer, HATCH ASSOCIATES, Mississauga, ON, Canada L5K 2R7. STAVROS ARGYROPOULOS (To whom correspondence should be addressed. E-mail: argyro@ecf.utoronto.ca), Professor, is with the Department of Metallurgy and Materials Science, University of Toronto, Toronto, ON, Canada M5S 3E4.

Manuscript submitted January 8, 1999.

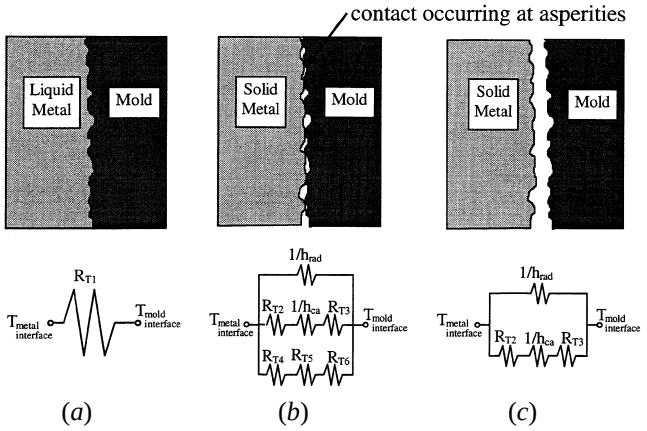

Fig. 1—(*a*) through (*c*) Development of the air gap at the metal-mold interface.

A. *Air Gap Formation and Heat Transfer at the Metal-Mold Interface*

Considerable attention has been given to measuring the formation of an air gap at the metal-mold interface during casting. Early techniques[1,2,3] relied on a variety of different strategies, including cooling curve inflections, capacitance sensors, and Vycor probes. Modern techniques for accurate air gap measurements[4–10] rely on the linear variable differential transformer (LVDT). Details into the development of the LVDT as an air gap measurement device are described elsewhere.[11] As air gap measurement techniques became well established, subsequent attention was directed to the mechanisms responsible for the drop in heat transfer. It was initially anticipated by Mackenzie and Donald[6] that the governing mechanism for heat transport across the gap was radiation. Ho and Pehlke[12] have shown that conduction and radiation (but not convection since the gap thickness and, hence, the Grashof number are minuscule) are both responsible, and, today, this is the generally accepted view.

Studies have been done for decades estimating the heat transfer coefficient in a variety of casting systems. Basic measurements were conducted by Kumar[13] with aluminum alloys and by Hao[14] with steel and iron for specific casting situations. The effect of certain variables on the heat loss at the metal-mold interface has also received some attention. El-Mahallawy[15,16] examined the effect of melt superheat and chill material on heat transfer, and Song[17] conducted similar studies by varying gap gas pressures and mechanical loads applied to the castings. Heat transfer coefficients have even been estimated during mold filling by Chiesa.[18]

B. *The Four Stages of Interfacial Heat Transfer*

Casting is intrinsically a transient process, and the mechanisms of heat transfer at the interface change during the solidification process. This can have significant ramifications for the modeler who fails to take these mechanism changes into account when estimating heat transfer coefficients. The changes can be outlined as occurring in stages as illustrated in Figure 1 with equivalent circuit diagrams. Note that when one speaks of an overall heat transfer coefficient, one is referring to a net coefficient incorporating the sum of all heat transfer mechanisms that determine heat flow from the outer surface of the metal to the inner surface of the mold. Stage I occurs immediately after liquid metal is poured into the mold and is shown in Figure 1(a). Here, the only mechanism of heat flow is conduction from the liquid metal to the mold wall. Note that an interfacial resistance R_{T1} may exist between the liquid and solid, although this term is usually very small for liquid metal-mold interfaces.

Stage II is characterized by the solidification of a thin shell of metal next to the mold wall, as in Figure 1(b). The mold and metal show intermittent contact at asperities, and the overall heat transfer scenario becomes quite complex. Heat flow from the metal to the mold occurs *via* three mechanisms, and because this flow will take the path of least opposition, the overall resistance occurs in parallel, as shown in the equivalent circuit of Figure 1(b). Explicitly, the mechanisms can be described as follows. The first mechanism is conduction through the contacting asperities. Here, R_{T4} is the resistance due to the thickness of the metal asperity (proportional to the conductivity of the metal and inversely proportional to the length of the path of heat flow through the metal asperity). R_{T5} is the thermal contact resistance at the asperity interface. R_{T6} is the resistance due to the thickness of the mold asperity (proportional to the conductivity of the mold and inversely proportional to the length of the path of heat flow through the mold asperity). The second mechanism is conduction through the air pockets in between the asperities. Here, h_{ca} is the equivalent heat transfer coefficient representing conduction through the air pocket (proportional to the conductivity of the gas in the gap and inversely proportional to the width of the pocket). R_{T2} and R_{T3} are the thermal contact resistances between the metal-air and air-mold, respectively, and can usually be neglected. The final mechanism is radiation, which occurs between the metal and mold wall, with h_{rad} representing the radiative heat transfer coefficient.

During stage II, the roughness that exists at the interface complicates the estimation of a heat transfer coefficient by using analytical equations. Some statistical expressions, such as those published by Sridhar,[19] Yovanovich,[20] and Schneider,[21] have been derived for the special case where two surfaces remain in contact under pressure with each other. In these studies, the heat transfer coefficient between two surfaces is defined as a function of the harmonic mean of the conductivities of the mold and metal, the pressure applied between the metal and the mold, the hardness of the metal and mold, and the roughness of the metal-mold interface:

$$h_{contact} = f(k_{harm\text{-}mean}, P_{contact}, \text{hardness}, \text{roughness}_{surface}) \quad [1]$$

As soon as the pressure between the surfaces drops to zero (and the slightest gap begins to form), the expressions are no longer suitable. This instant represents the start of stage III (Figure 1(c)).

Stage III occurs as the casting first pulls away from the mold wall forming an undivided air gap between metal and mold. Here, heat flow occurs *via* conduction through the air gap and radiation between the metal and mold surfaces. Though the metal and mold asperities are no longer in contact with each other, they still dictate the path of heat flow from metal to mold.

Finally, stage IV is arbitrarily defined as the stage where the gap grows to a size where the asperities, or surface roughness, can be effectively neglected in estimating the flow of heat. This distinction is important in defining the

analytical expressions that one is permitted to use to estimate the overall heat transfer coefficient during each stage. For real surfaces, the following analytical expressions are applicable:

$$\text{Stage I: } h = \frac{1}{R_{T1}} \quad [2]$$

$$\text{Stage II: } h = h_{\text{contact}} \text{ (as in Eq. [1])} \quad [3]$$

$$\text{Stage III: no expression available} \quad [4]$$

$$\text{Stage IV: } h = h_{\text{cond,gas}} + h_{\text{radiation}} \quad [5]$$

$$= \frac{k_{\text{air}}}{A} + \frac{\sigma(T^2_{\text{metal,int}} + T^2_{\text{mold,int}})(T_{\text{metal,int}} + T_{\text{mold,int}})}{\frac{1}{\varepsilon_{\text{metal}}} + \frac{1}{\varepsilon_{\text{mold}}} - 1} \quad [6]$$

Here, σ is the Stefan–Boltzman constant and ε is the emmisivity of the wall surface.

Alternatively, the assumption that the mold and metal are "perfectly flat" can be used to simplify the complexity of the problem. The following analytical expressions define the problem for a perfectly flat interface:

$$\text{Stage I: } h = \frac{1}{R_{T1}} \quad [7]$$

$$\text{Stage II: } h = h_{\text{contact}} \quad [8]$$

$$\text{Stage III and IV: } h = h_{\text{cond,gas}} + h_{\text{radiation}} \quad [9]$$

$$= \frac{k_{\text{air}}}{A} + \frac{\sigma(T^2_{\text{metal,int}} + T^2_{\text{mold,int}})(T_{\text{metal,int}} + T_{\text{mold,int}})}{\frac{1}{\varepsilon_{\text{metal}}} + \frac{1}{\varepsilon_{\text{mold}}} - 1} \quad [10]$$

Note that all stages, including stage III, can be characterized for flat surfaces. Neglecting the radiative component will not introduce significant error for low-temperature systems and small gaps.

II. SPECIFICATION OF EXPERIMENTAL APPARATUS

An experiment to correlate heat transfer coefficients to air gap size is really two separate experiments conducted at once. The first experiment requires an examination of the system on a "thermal" basis, and the second experiment considers the system on a "mechanical" basis. The key device for analyzing the system thermally is the thermocouple, and mechanically, it is the LVDT.

The diameters of the thermocouple wire and the sheaths used in this study were 0.05 and 0.254 mm, respectively. The thermocouples were contained within hairlike 304 stainless steel sheaths with AWG 30 to 0.254 mm o.d.s. K-type modules on the data acquisition board specified the numerical calibration relationships. In the present experiments, the time lag problem does not become an issue, because the thermocouples ultimately used possessed a minute wire diameter (AWG 44 to 0.050 mm), liquid metal has a high heat diffusivity (the ability to heat/cool a thermocouple tip quickly), and most importantly, the temperature transients experienced during casting are sufficiently small to ensure that no appreciable lag occurs. A second issue that requires consideration relates to the errors generated by the thermocouple at steady state. These errors include the manufacturer's limits of error for the thermocouple wire used, cold junction compensation error, the analogue-to-digital converter resolution (significant digits), and error generated by the conversion of thermocouple emf to temperature. The overall contribution of these errors can be estimated by examining the cooling curves at several known temperature calibration points. The data acquisition system was used to measure the melting points of pure water, pure tin, pure lead, and pure aluminum. Upon examining each of the cooling curves, the approximate error observed was seen to increase with higher temperatures. The anticipated error as a function of temperature was calculated by fitting a straight line through the plotted errors. Another source of error related to the use of thermocouples concerns the accurate placement of the thermocouple beads. Thermocouple bead placement error was minimized by specifying that the mold be manufactured within minimal tolerances ($\pm$0.2 mm for drilled holes). This tolerance was verified using a Mitutoyo Model CD-6BS digital caliper. The strategy of adopting minute diameter sheaths minimizes any error associated with thermocouple conduction, as suggested in the *NANMAC Temperature Handbook*.[22] In addition, because the thermocouples are only used to measure relative temperature differences, if a small error is present, it will be factored out when the difference in temperatures is calculated.

The two LVDTs used in this study were identical Schaevitz model 100DC-D LVDTs with nominal linear ranges of 6 mm using the manufacturer's recommended CALEX Model 21550 15VDC Power Supply. Four main sources of error were identified and properly quantified: nonlinearity error, stability error, resolution error, and relative connecting rod expansion error. The nonlinearity error for the Schaevitz model 100DC-E LVDT is 0.25 pct of full range (manufacturer's specifications), which corresponds to an error of $\pm$0.015 mm. The stability error relates to the excitation circuitry and was specified as 0.125 pct of full range (manufacturer's specifications), or $\pm$0.0075 mm. For the LVDT, the resolution error is only limited by the electronics used to carry signals to the data acquisition system. In our case, for a 14 bit A/D converter, this results in an error of about $\pm$0.00003815 mm, which is not in the vicinity for being a cause for concern. The relative connecting rod expansion error is estimated to be less than one one-hundredth of a millimeter.[11]

A. *Calculating Heat-Transfer Coefficients from Thermocouple Data*

In order to calculate heat transfer coefficients during casting, one of two techniques can be employed. The first technique involves measuring temperatures in the bulk mold and metal at various internal points and using an inverse technique to estimate the surface temperatures and temperature gradient. This is known classically as the inverse method.[23,24] The energy balance technique, alternatively, attempts to monitor the temperatures at the inner and outer surfaces of the interface and a short distance into the mold to calculate a gradient. By performing an approximate energy balance at the interface, for small Δr,

$$q_{\text{conv,int}} = q_{\text{cond,int}} \quad [11]$$

$$h_{\text{int}}(T_{\text{metal,int}} - T_{\text{mold,int}}) = k_{\text{mold}}\left(\frac{T_{\text{mold,int}} - T_{\text{mold,(int}-\Delta r)}}{\Delta r}\right) \quad [12]$$

$$h_{\text{int}} = \frac{k_{\text{mold}}}{\Delta r}\left(\frac{T_{\text{mold,int}} - T_{\text{mold,(int}-\Delta r)}}{T_{\text{metal,int}} - T_{\text{mold,int}}}\right) \quad [13]$$

In comparison, the inverse technique is very stable but is computationally more intensive and has a slower response time (since any heat change must penetrate to the first embedded thermocouple to be detected). The heat balance technique can be more erratic at times, yet it is very efficient and has a fast response to changes in heat flux. In this study, the heat balance technique is employed.

B. *General Experimental Procedure and Apparatus*

A graphite crucible was packed with solid slabs of metal and placed within a Bradely coreless induction furnace. The furnace was used to melt the metal and elevate its temperature to 800 °C for aluminum and aluminum alloys and 400 °C for pure tin. These superheats were specified relatively high to allow for sufficient time in transferring the liquid metal to the mold for pouring. Thus, the pouring temperature was assumed to be about 750 °C for aluminum and aluminum alloys and about 350 °C for tin. When the desired superheat was reached, the power of the induction furnace was turned off to minimize any electrical interference between the furnace and the data acquisition system. The graphite crucible was raised from the furnace using a pair of tongs and placed on the pouring pocket of the special tilt apparatus. The mold was filled immediately within about 3 seconds, and any transient mixing subsided within a second or two. The metal was allowed to cool for at least 250 seconds as the thermocouples and LVDTs collected data every 0.5 seconds. The analogue signals from the thermocouples and LVDTs were sent to a μMac-6000 data acquisition system[25] and ultimately to a PC host for permanent storage. The μMac-6000 contains its own dedicated CPU and is programmed *via* μMac Basic. The data acquisition system, with 14 bit resolution, was more than adequate for our purposes. The bottom of the mold was constructed with a thin base of the same material as the mold walls (to maintain uniform structural continuity during expansion), and ultralow thermal diffusivity insulation was placed immediately below the thin base (to supply a sufficient insulating effect).

Studies from the work of Vicente-Hernandez,[26] Bellet,[27] and Gunasegaram[28] indicated that experimental temperature and LVDT readings taken in a cylindrical mold, with a casting bound at the axis of symmetry, did not differ according to the θ angle (around the axis of the cylinder) for a given radial position. These studies employed multiple LVDT setups to confirm the radial symmetry of the cylindrical geometry. Thus, the preferred orientation was selected with both LVDTs on the same side of the casting, one slightly above the other. Three independent trials were conducted in the same metal-mold system in this study to further validate this assumption. In the worst case, symmetry error will not exceed the ratio of the pin diameter to the casting diameter, which translates to 0.75 cm/6 cm or 12.5 pct error for the sand mold and 0.5 cm/6 cm or 8.3 pct error for the graphite and copper molds.

The mold interior thermocouples were placed in precision drilled holes, with the mold interface thermocouple less than a millimeter from the inner mold wall. The holes drilled to house the thermocouples (and, hence, the thermocouples themselves) were of minimal diameter so as to cause the least possible disruption to the resulting thermal field in the mold wall. The technique used to properly place the thermocouple measuring the metal outer temperature

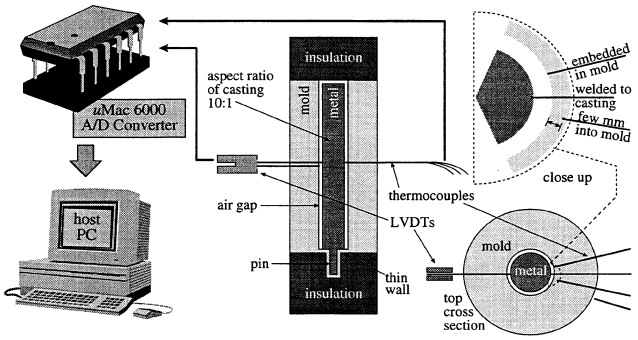

Fig. 2—Final experimental setup schematic.

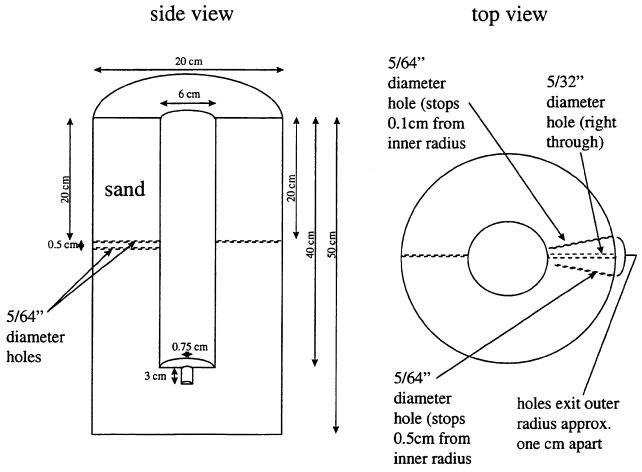

Fig. 3—Mold dimensions for sand casting.

required adopting a unique trick perfected after several trials. The thermocouple was passed into a hole drilled completely through to the inner wall of the mold cavity until the thermocouple tip protruded just enough into the mold cavity to allow the liquid metal to weld the tip to the outer wall of the casting. The thermocouple was allowed to slide freely so, as the casting contracts, it pulled the thermocouple with it. Here, the proper positioning of this thermocouple could be verified afterward *via* an inspection of the cast surface. The thermocouples were spring loaded to ensure that, as the mold expanded and contracted, intimate contact between the thermocouple and the mold would be maintained. A schematic of the final experimental setup is given in Figure 2.

For sand molds, the use of insulation was not practical (since sand is a good insulator itself). Thus, the dimensions of the mold were extended by a factor of 2 in the *z* direction. The mold dimensions for sand are given in Figure 3. The dimensions for graphite and copper molds are about half the height of those shown for sand with a 0.5-cm diameter pin hole, but otherwise are identical (*i.e.*, inner diameter of 6 cm, outer diameter of 20 cm, and height of 30 cm). The experimental trials were conducted without the use of washes at the mold inner surfaces. No welding occurred, as the aluminum did not readily diffuse into the copper wall during the time it was in its liquid state.

C. *Check for One Dimensionality of the System*

As mentioned previously, the requirement of one-dimensional heat flux radially outward is essential for obtaining

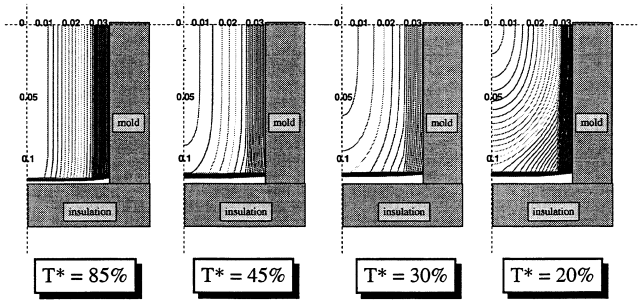

Fig. 4—Modeled cooling histories of a cylindrical casting.

Table I. Order of Experimental Trials

1	pure aluminum casting	graphite mold
2	pure tin casting	graphite mold
3	A356 aluminum casting	graphite mold
4	pure aluminum casting	sand mold
5	A356 aluminum casting	sand mold
6	pure aluminum casting	copper mold
7	A356 aluminum casting	copper mold
8	A206 aluminum casting	copper mold
9	aluminum 4 wt pct copper casting	copper mold

meaningful results. Eventually with time, despite efforts to change aspect ratios and insulate, end effects will cause the system to behave two-dimensionally. Ideally, one has a limited time in which to take temperature measurements, after which the data will begin to show appreciable departure from one-dimensionality. Usually, this can be seen when the normally monotonically decreasing value of the heat transfer coefficient starts to increase, but this is not a reliable measure by any means.

To solve this problem and estimate the duration of "one-dimensional conditions," a numerical model to the conduction problem in a cylinder considering only the thermal properties and the geometry of the metal-mold system was employed. The results for aluminum cast in a graphite mold are shown below in Figure 4, where

$$T^* = \frac{T - T_{\text{ambient}}}{T_{\text{initial}} - T_{\text{ambient}}} \qquad [14]$$

is the dimensionless average temperature of the casting, equal to 100 pct at initial pouring and equal to 0 pct at room temperature. Note that at $T^* = 85$ pct, the temperature isocontours are essentially vertical at the top axis of symmetry (where experimental measurements are taken), indicating that heat flow is radially outward, perpendicular to the isocontours. This pattern continues strongly until $T^* = 30$ pct, which is the last point where our 1D approximation is good. If one continues beyond this point, two-dimensional effects become apparent soon afterward at $T^* = 20$ pct, with a change in the slope of the temperature isocontours at the top axis of symmetry. For aluminum/graphite systems, this corresponds to about 500 seconds, which is reduced to 250 seconds to be completely safe.

III. EXPERIMENTAL RESULTS

The material combinations used in the experimental trials are given in Table I. The metals are essentially aluminum alloys, with tin used for comparison purposes. The molds were selected based on their average thermal diffusivities (equal to the mold thermal conductivity divided by the density and specific heat), which ranged from extremely high to very low (1.1×10^{-4} m^2/s for copper, 6.8×10^{-6} m^2/s for molded graphite from lampblack, and 6.6×10^{-7} m^2/s for green sand). Thermal diffusivity determines the type of temperature profile one would expect in the metal and the mold. This profile can range from cases where the casting can be treated as a lumped mass soon after pouring, as with sand molds, to cases where the gradients in the casting are greater than those in the mold, as with copper molds. Trials with A206 were accompanied by trials with a two-phase alloy, aluminum 4 wt pct copper (similar to A206), for comparison. The surface roughness of the molds was estimated as 1.5 μm for copper, 5 μm for graphite, and 500 μm for sand.[29,30,31]

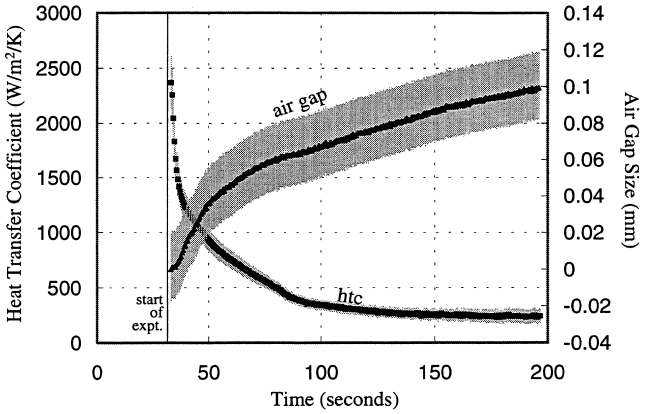

Fig. 5—Heat transfer coefficient and air gap size measurements for the aluminum-graphite system.

A. *The Aluminum-Graphite System*

The first system considered was the aluminum graphite system. In Figure 5, a combination plot of the measured variables during the early stages of the casting is shown; one can note the inverse relationship between the air gap size increase and the overall drop in the heat transfer coefficient. Initially, the drop in the coefficient is steep during the formative stages of the gap. This suggests that the heat flux from the casting is sharply reduced from the moment the air gap forms at the transition from stage II to stage III. Subsequent increases in the air gap size continue to decrease this heat flux but not with the same intensity as at the moment of initial formation. This observation makes perfect sense because the extreme insulating nature of air will naturally show an immediate jump in resistance to heat flow through the gap, even at very small thickness, and a slower increase in resistance with a change in thickness during stage III.

In Figure 6, the magnitude of the heat transfer coefficient is plotted against the size of the air gap, and the analytical solution for a perfectly flat interface based on Eqs. [7] through [10] is shown for comparison. The analytical expressions adopt the temperature varying thermal conductivity of air[32] and the emmisivities of each metal and mold surface. The experimental curve can be broken into three zones of different slope from stages II to IV. Stage II involves a sharp

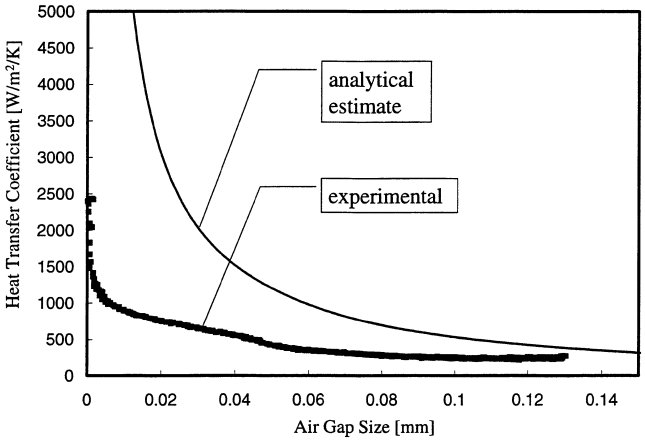

Fig. 6—Heat transfer coefficient–air gap size correlation for the aluminum-graphite system.

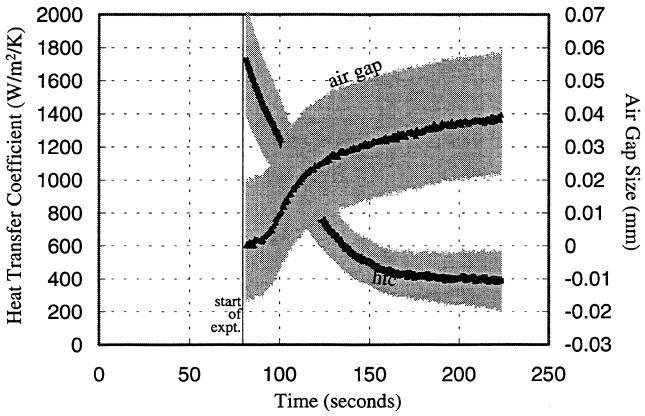

Fig. 7—Heat transfer coefficient and air gap size measurements for the A356-graphite system.

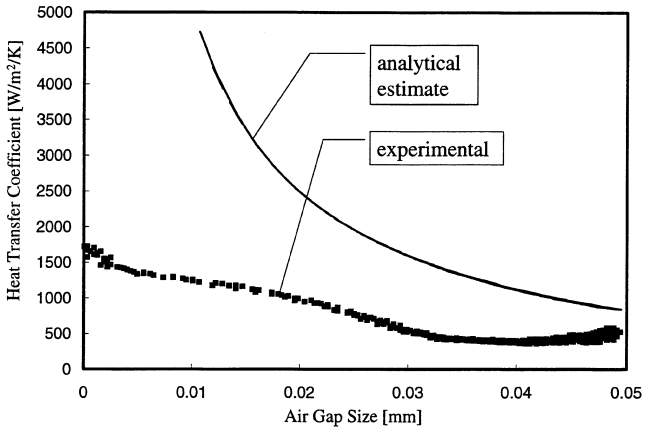

Fig. 8—Heat transfer coefficient–air gap size correlation for the A356-graphite system.

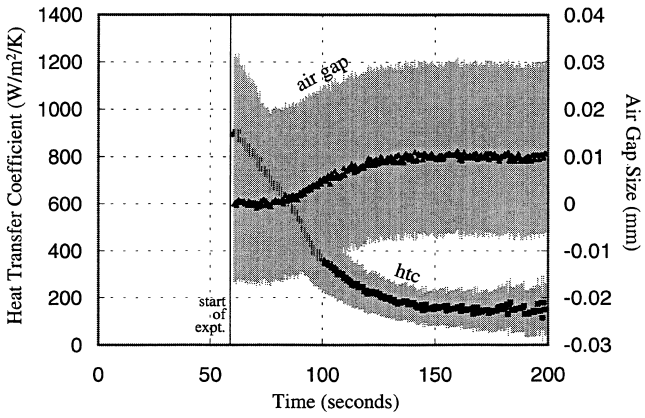

Fig. 9—Heat transfer coefficient and air gap size measurements for the tin-graphite system.

drop in heat transfer coefficient before the air gap has begun to form. Resistance to heat flow increases greatly despite no appreciable gap formation. Here, the contact heat transfer coefficient term h_{contact} in Eq. [3] can be thought to be progressively decreasing. Equation [7] for perfect surfaces approaches infinity as the air gap approaches zero. For real surfaces, this limit is never reached, and the roughness present between real surfaces will prevent Eq. [7] from predicting a representative value for the heat transfer coefficient. The transition from Eq. [2] to [4] for a real surface will occur not at an instant, but over a range, which can be observed as a change in the slope of the curve in Figure 6 as the air gap grows from a minute size to about 0.06 mm. This transition zone represents stage III.

During stage III, it is believed that two competing factors are most influential in altering the magnitude of the heat transfer coefficient at the interface: the thickness of the air gap and the degree of surface roughness relative to the air gap size. The air gap size has an inverse effect on the heat transfer coefficient, and the roughness has an effect that is strongest at extremely small gap sizes and diminishes as the gap size becomes larger. This trend is evident in Figure 6 as the difference between experimental and analytical solutions is seen to diminish with increasing air gap size.

The curve appears to enter stage IV at larger gap sizes ($>$0.06 mm). The "roughness aspect ratio" (the size of the surface roughness peaks relative to the magnitude of the air gap) no longer changes as drastically as it did when the air gap size approached zero. Thus, the transient effect of roughness becomes more and more negligible for larger air gap sizes as the surfaces behave more and more as "perfectly flat" surfaces. If the air gap continues to grow, it will eventually reach a magnitude where the roughness of the surfaces can be neglected, and Eq. [5] can be used to estimate the heat transfer coefficient more accurately. This study will concern itself with characterizing the heat transfer coefficient at times when the surface roughness cannot be neglected. The three-zone change in slope pattern has also been observed by other researchers, Gunasegaram[28] and Bellet,[27] in other metal-mold systems. For each correlation plot in this study, the slope of the curve during stage II is greater than during stage III, which in turn, is greater than during Stage IV.

The equivalent plots for each metal-mold system are given in Figures 7 through 23. In graphite molds, A356 exhibits different solidification/air gap formation behavior than pure aluminum; most of that behavior difference can be attributed to the existence of a mushy zone and to the fact that A356 experiences less thermal contraction than pure aluminum. Tin was the only nonaluminum casting material examined, chosen for its tendency to form small air gaps, as seen in Figure 9. Notwithstanding this scatter, upon closer examination, one is able to distinguish the stages here as well in the

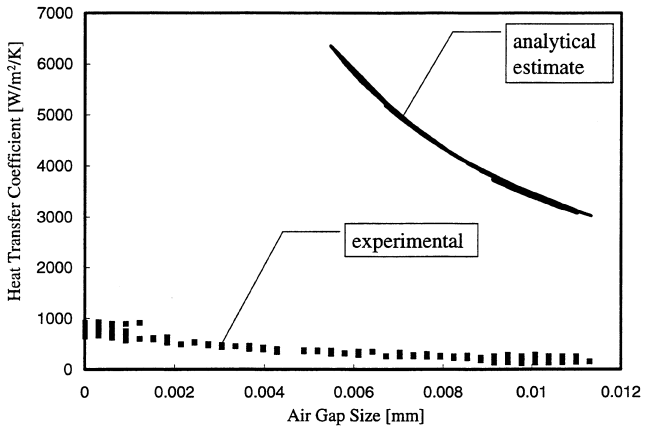

Fig. 10—Heat transfer coefficient–air gap size correlation for the tin-graphite system.

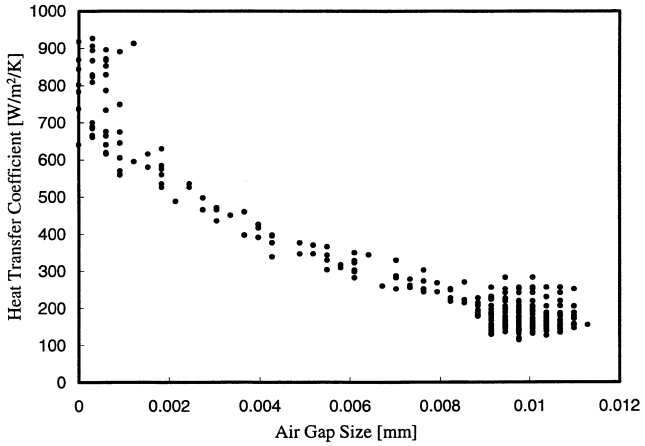

Fig. 11—Closeup of heat transfer coefficient–air gap size correlation for the tin-graphite system.

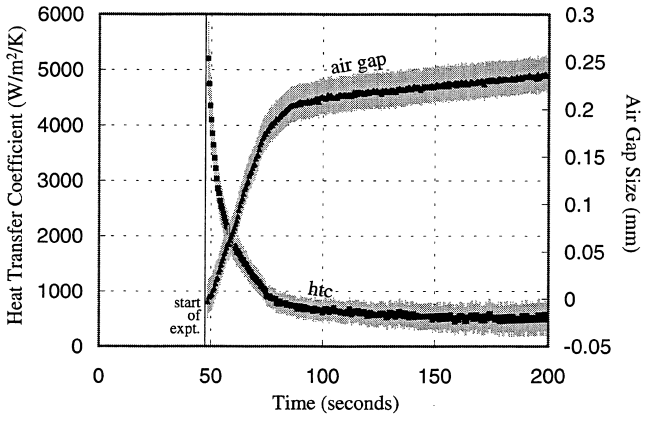

Fig. 12—Heat transfer coefficient and air gap size measurements for the aluminum-copper system, trial I.

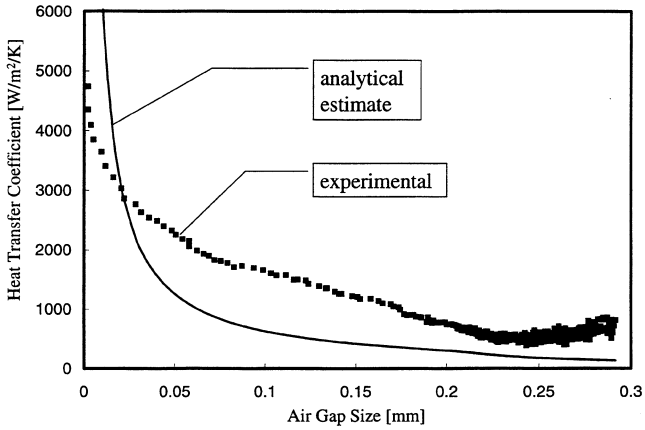

Fig. 13—Heat transfer coefficient–air gap size correlation for the aluminum-copper system, trial I.

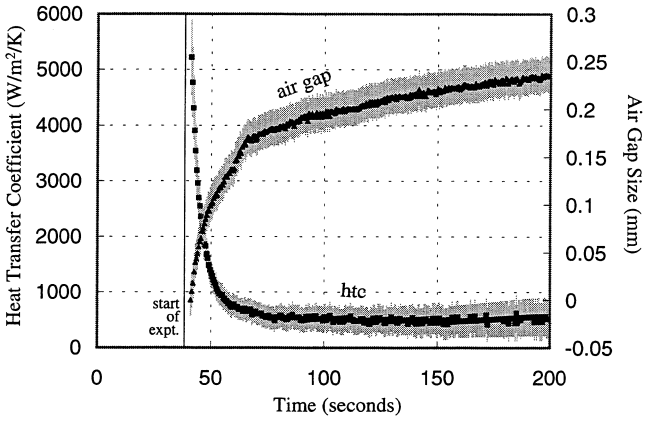

Fig. 14—Heat transfer coefficient and air gap size measurements for the aluminum-copper system, trial II.

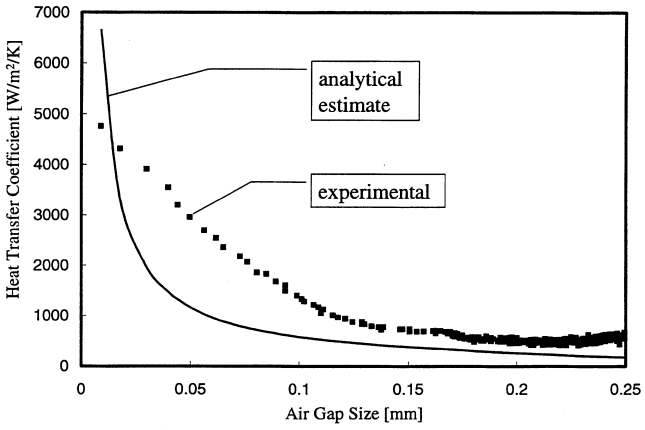

Fig. 15—Heat transfer coefficient–air gap sizes correlation for the aluminum-copper system, trial II.

closeup plot of Figure 11. The size of the air gap remains small so only stages II and III are observed. Therefore, the analytical curve (stage IV) is completely inadequate in predicting the heat transfer coefficient, as is obvious from Figure 10.

In copper molds, the three trials conducted with pure aluminum produced highly repeatable data. In each trial, the difference between experimental data and the analytical expression is drastically reduced compared to the graphite mold trials. This is a logical observation, since the average roughness of polished copper (1.5 μm) was over an order of magnitude smaller than the average roughness of the graphite (20 μm). Similar differences to those observed

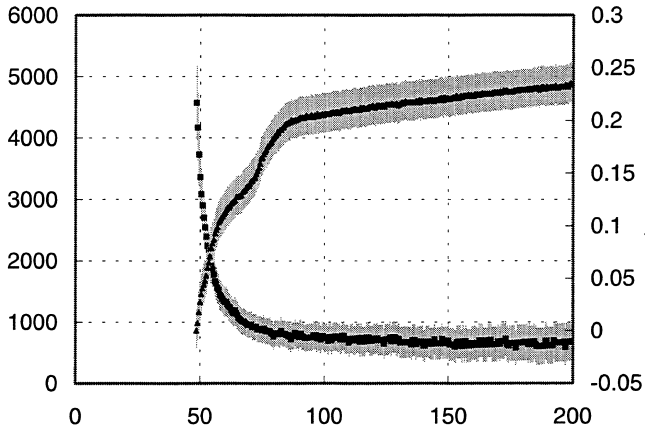

Fig. 16—Heat transfer coefficient and air gap size measurements for the aluminum-copper system, trial III.

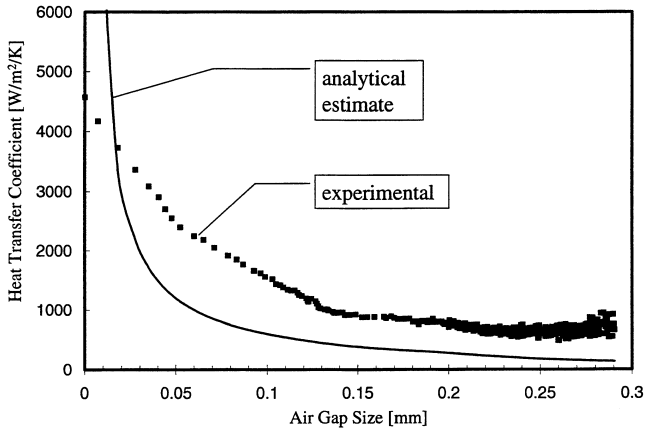

Fig. 17—Heat transfer coefficient–air gap size correlation for the aluminum-copper system, trial III.

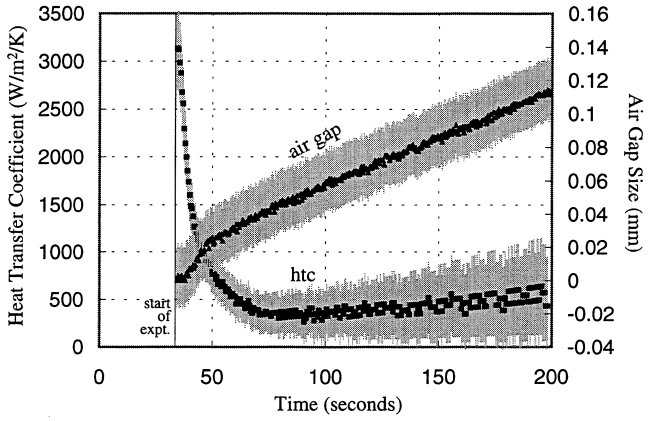

Fig. 18—Heat transfer coefficient and air gap size measurements for the A356-copper system.

between A356 and pure aluminum cast in graphite molds were also evident between pure aluminum and the alloys in copper molds. This difference may again be attributed to the mushy zone effect in alloys and higher error than in the pure aluminum-copper system.

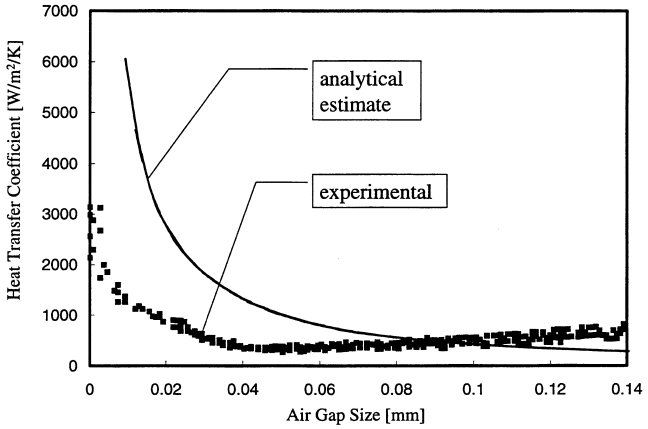

Fig. 19—Heat transfer coefficient–air gap size correlation for the A356-copper system.

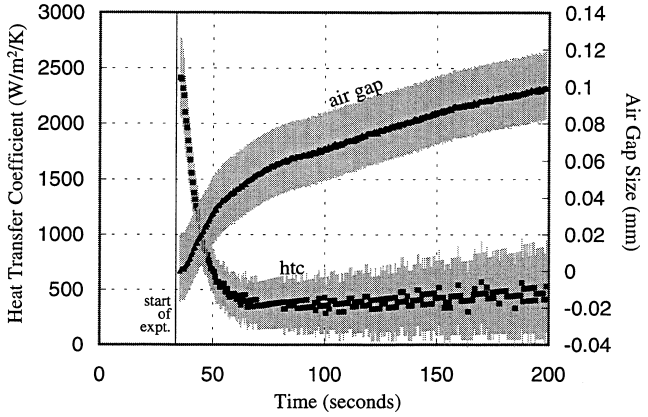

Fig. 20—Heat transfer coefficient and air gap size measurements for the A206-copper system.

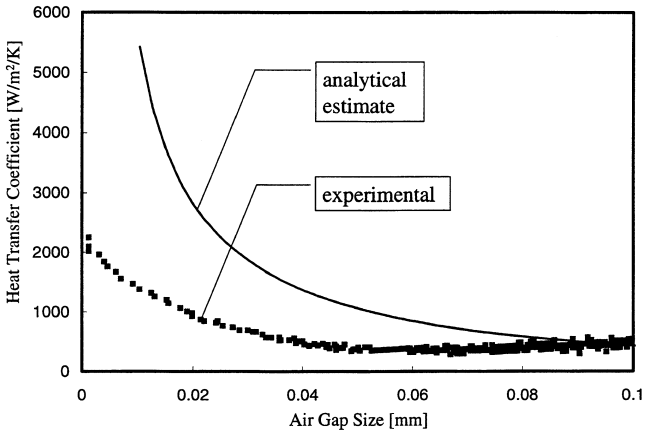

Fig. 21—Heat transfer coefficient–air gap size correlation for the A206-copper system.

IV. CORRELATION DEVELOPMENT

The heat transfer coefficient at the metal-mold interface of a solidifying casting contracting from the mold wall is a function of several parameters, as shown in Figure 24. The width of the air gap is the most dominant variable and has been stressed up to this point. Additionally, the thermophysical properties of the metal and the mold can affect the

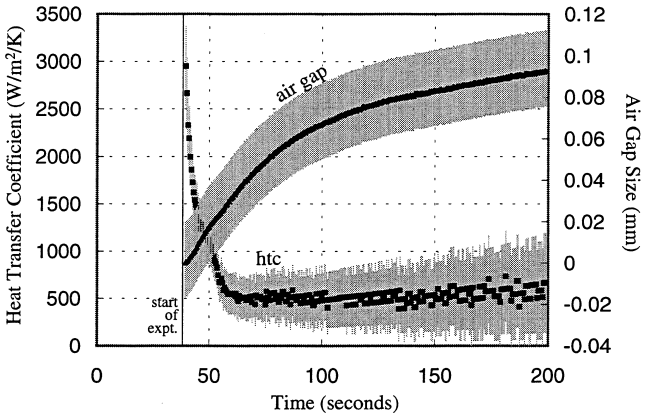

Fig. 22—Heat transfer coefficient and air gap size measurements for the 4 wt pct Cu aluminum-copper system.

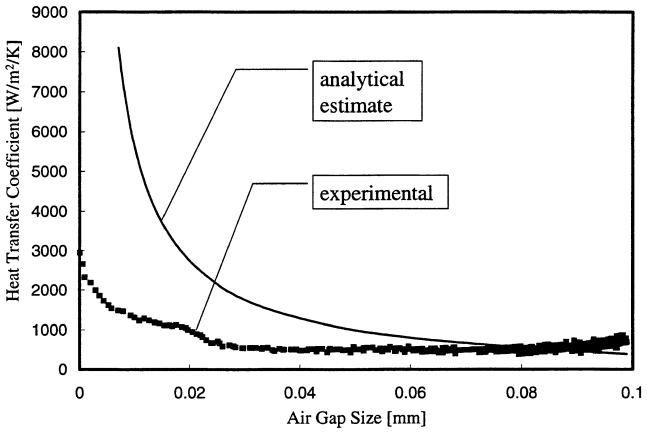

Fig. 23—Heat transfer coefficient–air gap size correlation for the 4 wt pct Cu aluminum-copper system.

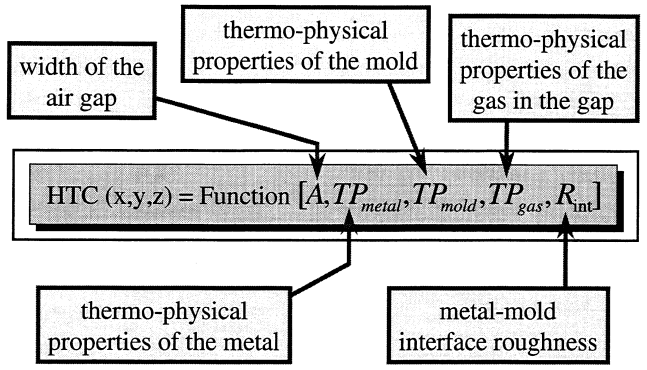

Fig. 24—Most significant variables affecting the heat transfer coefficient at the metal-mold interface during casting.

equivalent heat transfer coefficient in two ways. First, the metal and mold thermo-physical properties influence the temperature of the metal and the mold interfaces at any given time during solidification. The temperatures of these interfaces can affect the thermophysical properties of the gas in the gap causing heat to flow out of the mold at different rates. Second, a change in surface temperatures will influence the rate at which heat is lost *via* radiation. This effect will become increasingly influential only at higher temperatures because heat flux due to radiation varies to the fourth power of temperature. The effect of thermophysical properties on the proposed general correlation is discussed in detail in Part II of this study. Radiation constitutes a maximum of about 5 pct of the overall heat transfer coefficient value in aluminum castings and far less in tin, so it can safely be neglected in these systems. The thermophysical properties of the gas in the gap (or, more importantly, the conductivity) will greatly influence the heat transfer coefficient, as heat will *conduct* through the gap from metal to mold surfaces. The influence of this variable is not explored in the present study, since all of the work is conducted with a single gap gas, *i.e.*, air. The thermophysical property variation of air with temperature, however, is considered.

The metal-mold interfacial roughness, a measure of the initial roughness of the mold inner wall prior to casting, will further effect the heat transfer coefficient. Initially, when the mold and metal surfaces are in contact, the roughness of the metal-mold walls can add considerably to the equivalent resistance of the interface. After a gap begins to form, roughness will still have an important effect, as rough "peaks" jutting out of either the metal or the mold will act as fins, distorting the paths available for the flow of heat. This effect is accounted for in Part II.

Other variables that can generally influence the heat transfer coefficient (but can be neglected in the metal-mold systems examined in this study) include the emmisivities and hardness of the mold and metal walls and the pressure at the metal-mold interface. The emmisivities become influential in higher temperature systems, such as steel castings, where the radiative component of the heat transfer coefficient is significant. The hardness of the metal and mold walls and the pressure at the interface will become influential only in cases where the mold and metal surfaces contract toward each other (*i.e.*, at mold cores), and no air gap forms.

Though the magnitude of the air gap size undoubtedly plays a dominant role in determining the overall heat transferred from metal to mold (because it represents the greatest single source of resistance), neglecting the effect of the other variables can render comparative studies ineffective. Casting in a hydrogen environment, for example, instead of air can increase the heat transfer coefficient fourfold, as noted by Campbell.[33] Indeed, a patent already exists for this process. Whereas unwanted variables can be kept constant for a particular trial, a set of correction factors is needed to extend results to other systems where these variables change significantly.

B. *Correlation of Experimental Data*

Having established the most general form of the equation for the heat transfer coefficient at the interface as

HTC = function (air gap size, roughness of mold surface, conductivity of gas in the gap, thermophysical properties of the metal, thermophysical properties of the mold, emmisivity of the metal and mold walls, hardness of the metal and the mold, contact pressure at the metal-mold interface) [15]

and, by neglecting the variables that are not influential for

low-temperature (< 800 °C) casting process where a gap forms, this equation reduced to

HTC = function (air gap size, roughness of mold surface, conductivity of gas in the gap, thermophysical properties of the metal, thermophysical properties of the mold) [16]

A specific functional form for the relationship can be formulated to correlate both experimental data from the present study and data available in the literature. Unfortunately, the literature data did not include all of the essential variables of Eq. [16] for comparison. As a result, the correlations developed in this section will adopt a semiempirical relationship based on the dominant variable of interest, the air gap size. The relationship will allow comparisons to be made between a wide variety of studies. Part II will present a more general analysis based on the complete set of defined variables in Eq. [16]. The form of the equation was chosen as

$$\text{HTC} = \frac{1}{k \cdot A + r} + C \qquad [17]$$

Though partially empirical, Eq. [17] can be used to bridge the void in estimating HTC between stages II and IV described by Eqs. [3] through [6]. Since stage III cannot be mathematically defined, Eq. [17] serves to approximate the transition between stages II and IV by approaching Eq. [3] for stage II as A approaches 0 and Eq. [6] for stage IV as A approaches infinity. The equation accommodates the dominant air gap size variable and allows for variations in roughness, radiation, and other uncontrolled variables present between differing literature studies to be "absorbed" by the k, r, and C constants. The greater the effects of these variables, the more the constants k, r, and C will differ from trial to trial.

The variables k, A, r, and C are input with the units W^{-1} m^2 K mm^{-1}, mm, W^{-1} m^2 K, and W m^{-2} K^{-1}, respectively. The coefficients r and C can be negative in the correlation because these values represent the "calibration" parameters used to fix the inverse relationship to its maximum (initial) and minimum (final) values. The coefficient k must never be negative because this parameter determines the influence of an increase in air gap size on the resulting heat transfer coefficient. A negative k value would imply the heat transfer coefficient is increasing with an increase in air gap size.

The correlations from the experimental work of this study are presented in Figures 25 through 31 and are summarized with respect to previous literature studies in Table II. The values in bold were obtained from data in the literature. The results from many of these experimental trials indicate that the value of heat transfer coefficients and air gaps measured can vary substantially from trial to trial where experimental procedures are not conducted in a consistent fashion. Equivalent measurements in three-dimensional systems are further complicated by several factors, including a superposition of effects in the vicinity of adjacent walls and the need for precise tracking of the air gap along each metal-mold interface. The use of a numerical model becomes essential with these complicated geometries.

V. SUMMARY AND CONCLUSIONS

In this study, an investigation to determine the most influential factors responsible for inducing a change in the cooling rate of a casting was undertaken. The formation of an air gap at the metal-mold interface was isolated as the most significant variable, and a systematic approach (not limited to a specific industrial process) was undertaken to quantify the heat transfer coefficient–air gap relationship across a varying range of molds with varying thermophysical properties and surface roughness. The experimental work necessary for implementing the boundary condition coupling strategy

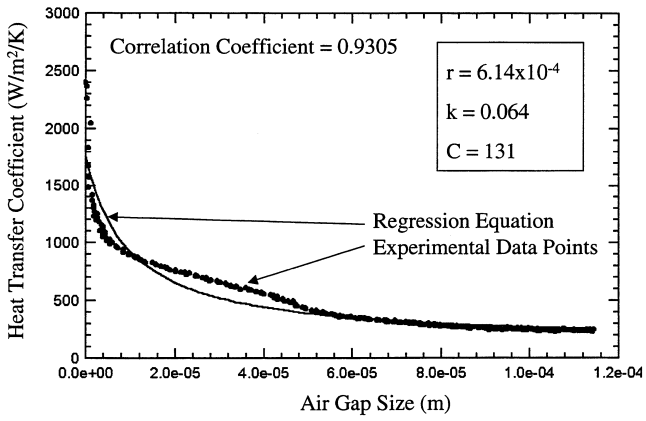

Fig. 25—Correlation plot for commercial purity aluminum cast in a graphite mold.

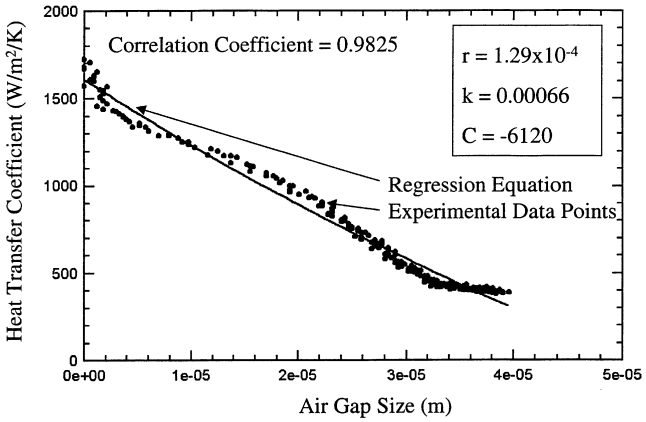

Fig. 26—Correlation plot for A356 aluminum alloy cast in a graphite mold.

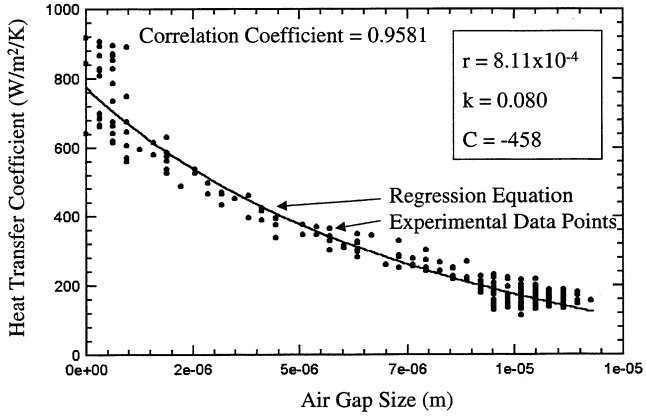

Fig. 27—Correlation plot for pure tin cast in a graphite mold.

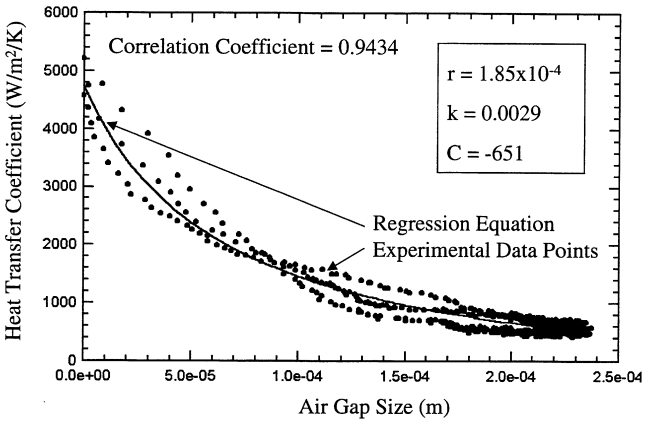

Fig. 28—Correlation plot for commercial purity aluminum cast in a copper mold.

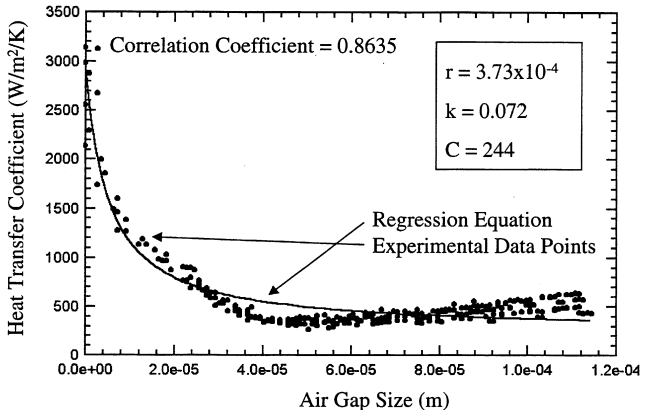

Fig. 29—Correlation plot for A356 aluminum alloy cast in a copper mold.

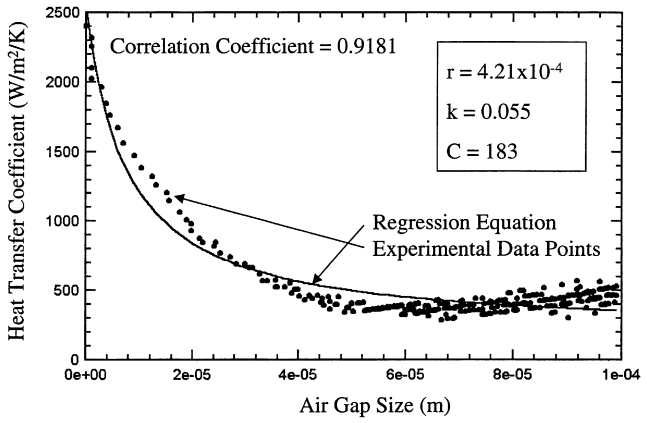

Fig. 30—Correlation plot for A206 aluminum alloy cast in a copper mold.

was described, and it was observed that heat transfer coefficients and air gap sizes could be more accurately measured using experimental techniques designed and optimized in this study.

Error analysis was used to confirm the reliability of the experimental results and identify significant limitations. The expected inverse relationship between the wall heat transfer coefficient and the air gap was observed for all metal-mold systems. Also noted was the intense reduction in the overall

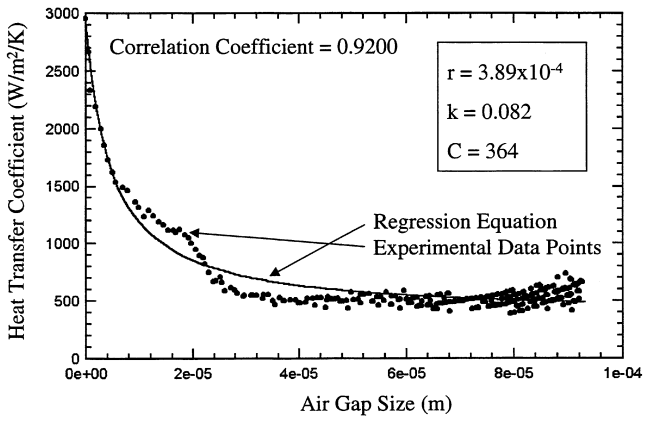

Fig. 31—Correlation plot for A1-4 wt pct Cu aluminum alloy cast in a copper mold.

heat flux out of the casting with the initial formation of the air gap, an important consideration for mold designers. A semiempirical inverse equation of the form htc = $[(1/k \cdot A + r) + C]$ was found to best characterize the relationship between the heat transfer coefficient and air gap for all metal-mold systems considered. This equation accounted for the uncertainty present when the surface roughness asperities are of similar magnitude to the air gap size. Previous comparable documented studies had relied on at least three different straight-line segments, fit from data obtained by means of a process specific experimental setup. The general heat transfer coefficient equation was also applied to data from the literature, and it was determined that this inverse function was able to accurately describe the relationship. Part II of this study will apply the findings of this work to complete the coupling strategy.

NOMENCLATURE

A	air gap width in air gap correlations, mm
C	constant in the air gap correlations, W m^{-2} K^{-1}
E	expansion rod error, m
h	heat transfer coefficient, W m^{-2} K^{-1}
htc (HTC)	heat transfer coefficient, W m^{-2} K^{-1}
k	conductivity, W m^{-1} K^{-1} or conductivity related parameter in the air gap correlations, W^{-1} m^2 K mm^{-1}
L	nonlinearity error, m
M	any variable of interest
P	pressure, N m^{-2}
r	r coordinate or resistivity related parameter in the air gap correlations, W^{-1} m^2 K
R	thermal resistance, W^{-2} m^2 K (for the heat transfer equations) or A/D resolution error, m
S	stability error, m
T	temperature, K
x	x coordinate

Greek Symbols

ε	emmisivity (for the heat transfer equations)
σ	Stefan–Boltzman constant, 5.67051×10^{-8} W m^{-2} K^{-4}

Table II. Summary of Experimental Results and Correlations

System Metal/ Mold*	$h_{maximum}$ (W m^{-2} K^{-1})	$h_{minimum}$ (W m^{-2} K^{-1})	Maximum Gap (mm)	Stage II Effectiveness of Eq. [17] at $A = 0$	Stage III Effectiveness of Eq. [17] at Int. A	Stage IV Effectiveness of Eq. [17] at Large A
Al/graphite	2400	250	0.1	good	good	good
A356/graphite	1700	400	0.04	good	good	poor
Sn/graphite	900	170	0.01	good	good	good
Al/copper	5000	600	0.25	good	good	fair
	5000	**2000**	**0.03**	**poor**	**good**	**poor**
	2400	**100**	**4.6**	**good**	**good**	**poor**
*coating	**3200**	**200**	**0.05**	**poor**	**good**	**good**
A356/copper	3200	500	0.12	good	good	good
A206/copper	2500	400	0.1	good	good	good
Al-4 pct wt Cu/copper	2800	400	0.1	good	good	good
Al alloy/copper	**8000**	**1000**	**0.015**	**good**	**good**	**good**
Al alloy/copper* coating	**3000**	**400**	**0.07**	**good**	**good**	**fair**
Al alloy/steel	**400**	**100**	**0.5**	**fair**	**good**	**poor**
Al alloy/steel	**260**	**100**	**0.37**	**good**	**good**	**poor**
Al alloy/steel	**10000**	**1700**	**0.03**	**poor**	**good**	**good**

* Data in bold indicate values derived from the literature data.

Subscripts

cond	conduction
conv	convection
harm	harmonic
i	*i*th direction, coordinate
int	interface
T1 through T6	identifiers for thermal resistance terms

Superscripts

*	dimensionless

REFERENCES

1. J. Savage: *J. Iron Steel Inst.*, 1962, vol. 200, pp. 41-57.
2. J. Majumdar, B.C. Raychaudhuri, and S. Dasgupta: *Int. J. Heat Mass Transfer*, 1981, vol. 24(7), pp. 1089-95.
3. B.P. Winter, T.R. Ostrom, T.A. Sleder, P.K. Trojan, and R.D. Pehlke: *AFS Trans.*, 1987, vol. 93, pp. 259-66.
4. J. Issac, G.P. Reddy, and G.K. Sharma: *Inst. Ind. Foundrymen*, 1984, vol. 33, pp. 15-19.
5. Y. Nishida, W. Droste, and S. Engler: *Metall. Trans. B*, 1986, vol. 17B, pp. 833-44.
6. I.M. Mackenzie and A. Donald: *J. Iron Steel Inst.*, 1950, vol. 166, pp. 19-24.
7. D.M. Lewis and J. Savage: *Met. Rev.*, 1956, vol. 1, pp. 65-78.
8. C. Lukens, T.X. Hou, and R.D. Pelke: *AFS Trans.*, 1990, vol. 98, pp. 63-70.
9. D. Pehlke: in *Modeling of Casting Welding, and Advanced Solidification Processes—VII*, TMS, Warrendale, PA, 1995, pp. 373-380.
10. V. Sahai and R.A. Overfelt: in *Modeling of Casting, Welding, and Advanced Solidification Processes—VII*, TMS, Warrendale, PA, 1995, pp. 417-24.
11. M. Trovant: Ph.D. Thesis, University of Toronto, Toronto, 1998.
12. K. Ho and R.D. Pehlke: *AFS Trans.*, 1984, vol. 61, pp. 587-98.
13. T.S. Prasanna Kumar and K. Narayan Prabhu: *Metall. Trans. B*, 1991, vol. 22B, pp. 717-27.
14. S.W. Hao, Z.Q. Zhang, J.Y. Chen, and P.C. Liu: *AFS Trans.*, 1987, vol. 95, pp. 601-08.
15. N.A. El-Mahallawy and A.M. Assar: *J. Mater. Sci.*, 1991, vol. 26, pp. 1729-33.
16. M.A. Taha, N.A. El-Mahallawy, A.M. Assar, and R.M. Hammouda: *J. Mater. Sci.*, 1992, vol 27, pp. 3467-73.
17. S. Song, M.M. Yovanovich, and K. Nho: *J. Thermophys.*, 1992, vol. 6(1), pp. 62-68.
18. F. Chiesa: *AFS Trans.*, 1990, vol. 98, pp. 193-200.
19. M.R. Sridhar and M.M. Yovanovich: *J. Thermophys. Heat Transfer*, 1994, vol. 8, pp. 633-40.
20. M.M. Yovanovich: *Heat Transfer Vol. 1*, Hemisphere, New York, NY, 1986.
21. P. J. Schneider: in *Handbook of Heat Transfer*, McGraw-Hill, New York, NY, 1973.
22. *NANMAC Temperature Handbook*, NANMAC Corp., Framingham, MA, 1989.
23. Y. Ruan, J.C. Liu, and O. Richmond: *Inv. Prob. Eng.*, 1994 vol. 1, pp. 45-69.
24. P.G.Q. Netto, R.P. Tavares, and R.I.L. Guthrie: *Proc. 36th Int. Symp.: Light Met.*, CIM, Sudbury, 1997, pp. 393-407.
25. *μMac-6000 Operations, Concepts, Command References, Programming and Users Manual*, Analog Devices Inc., Norwood, MA, 1988.
26. P. Vicente-Hernandez, F. Decultieux, P. Schmidt, L. Svensson, and C. Levaillant: *Iron Steel Inst. Jpn. Int.*, 1995, vol. 35, pp. 805-12.
27. M. Bellet, F. Decultieux, M. Menai, F. Bay, C. Levaillant, J.L. Chenot, P. Schmidt, and I.L. Svensson: *Metall. Trans. B*, 1996, vol. 27B, pp. 81-99.
28. D.R. Gunasegaram, D. Celentano, and T.T. Nguyen: *Proc. Int. Symp. on Application of Sensors & Modeling in Materials Processing II*, TMS Annual Meeting, Feb. 9–13, Orlando, FL, 1997.
29. *ASM Handbook*, vol. 5, Surface Engineering, ASM INTERNATIONAL, Materials Park, OH, 1996.
30. T.R. Thomas and M.I. Prode: *Rough Surfaces*, Longman Publishing, London, 1982.
31. J.M. Bennett and L. Mattsson: *Introduction to Surface Roughness and Scattering*, Optical Society of America, Washington, DC, 1989.
32. N.V. Suryanarayana: *Engineering Heat Transfer*, West Publishing Co., Los Angeles, CA, 1995.
33. J. Campbell: *Mater. Sci. Technol.*, 1991, vol. 7, pp. 885-94.